https://doi.org/10.1016/j.tws.2021.107858

Experimental and numerical studies on stress concentration factors of high strength steel fabricated box X-joints

Xiaoyi Lan[a,*], Tak-Ming Chan[b], Ben Young[b]

[a] School of Civil and Environmental Engineering, Nanyang Technological University, Singapore

[b] Dept. of Civil and Environmental Engineering, The Hong Kong Polytechnic University, Hong Kong, China

*xiaoyi.lan@connect.polyu.hk

Abstract: High strength steel (HSS) is commonly available in the form of steel plates. The built-up box tube with sharp corners which is welded from four steel plates is usually fabricated for construction. The stress concentration factor (SCF) is crucial for the determination of the hot spot stress range which governs the high-cycle fatigue resistance of tubular joints. This paper presents experimental and finite element (FE) investigations on the SCF of HSS fabricated box X-joints. Four X-joints which are fabricated from built-up box tubes with a nominal yield stress of 890 MPa are tested under brace axial compression. The SCFs at typical hot spot locations are obtained using strip strain gauges. A FE model which has been validated against the test results is employed to conduct the parametric study on totally 112 fabricated box X-joints. The loading cases of brace and chord axial loading are covered. The effects of brace to chord width ratio, chord width to wall thickness ratio and brace to chord wall thickness ratio on the SCFs at the hot spot locations are revealed. The CIDECT SCF formulae are shown to be not suitable for the fabricated box X-joints under brace and chord axial loading. More accurate SCF equations are proposed to calculate the SCFs at the hot spot locations of the box X-joints.

Keywords: Axial loading; Box X-joint; Fatigue design; High strength steel; Stress concentration factor

1. Introduction

Numerous tubular structures which are widely used in onshore and offshore structures (e.g. bridges, mobile cranes, wind turbines and offshore platforms) are subjected to fatigue loading. The prolonged time-variant fatigue loading could result in crack initiation, subsequent crack growth and eventually fracture failure of tubular joints which are critical components in tubular structures [1]. This could lead to the collapse of tubular structures due to the fatigue failure of tubular joints, and therefore corresponding fatigue design rules for tubular joints are needed.

The International Institute of Welding (IIW) proposed the IIW recommendations [2] for the fatigue design of tubular joints. The design recommendations are based on reported results of extensive test and finite element (FE) studies on normal strength steel tubular joints. The IIW recommendations [2] forms the basis of many international design standards and design guides e.g. the ISO 14347 [3] and the CIDECT design guide No. 8 [4]. The hot spot stress method which relates the high-cycle fatigue resistance (i.e. the number of cycles to fatigue failure) to the hot spot stress range is used for the fatigue design [2-4]. The hot spot stress is the maximum geometrical stress occurring in a joint. The stress concentration factor (SCF) which is defined as the ratio of hot spot stress range in a joint to the nominal stress range in the chord or brace member is used to facilitate the determination of hot spot stress range for designers. It should be noted that the codified fatigue design rules [2-4] are stipulated for cold-formed and hot-finished rectangular hollow section (RHS) joints with round tube corners. Meanwhile, the popularity of high strength steel (HSS) with yield stresses higher than 450 MPa is increasing in tubular structures. However, HSS is commonly available in the form of steel plates. The corner cracking can occur during the cold-forming process of HSS sections because of its lower material ductility [5]. The HSS fabricated box tube which is directly welded from four steel plates can avoid the corner cracking. The box tube is also preferred in heavy-loaded tubular structures. HSS fabricated box tubes with sharp tube corners are thus commonly fabricated and employed for construction.

Recent research advances of SCFs of tubular joints have been made mostly for cold-formed and hot-finished steel tubular joints. SCF formulae have been proposed for uniplanar tubular joints by, among others, Feng and Young [6], Daneshvar et al. [7-8] and Matti and Mashiri [9-10] for RHS X- and T-joints; Li et al. [11] and Cheng et al. [12] for bird-beak square hollow section (SHS) X-joints; Chen et al. [13], Feng et al. [14] and Xu et al. [15] for K-joints. The SCFs of multiplanar tubular joints have also been addressed by e.g. Ahmadi and Kouhi [16] for multiplanar XT-joints, Jiang et al. [17] for multiplanar DT-joints and Bao et al. [18] for multiplanar Y-joints. In contrast, corresponding research on the fabricated box joints remains limited. Jiang et al. [19] and Chiew et al. [20] experimentally examined the SCF distribution and fatigue performance of fabricated box T-joints with a nominal yield stress of 690 MPa. It is found that the highest SCF occurred at the corner on the chord weld toe, and the CIDECT fatigue design rules are conservative for the test specimens. Jiang et al. [21-22] proposed SCF equations for concrete-filled fabricated box X- and Y-joints. However, the suitability of the codified design rules for the fabricated box X-joints with sharp tube corners remains unclear. For one specified joint configuration, the SCFs are mainly governed by the loading types, joint geometric parameters and elastic material properties of steel, and the SCFs can vary largely for different joint configurations. It may be intuitive to categorise

the cold-formed/hot-finished SHS X-joints and the fabricated box X-joints as the same joint type. It is noted that the SCFs are sensitive to the detailed joint configurations. The sharp tube corners in fabricated box X-joints can alter the stress distribution and thus affect the SCFs and fatigue performance when compared with the cold-formed and hot-finished counterparts. The brace axial loading and chord axial loading are basic loading types for tubular structures e.g. the offshore platforms under the fatigue loading from waves and wind. Research on the SCFs of the fabricated box X-joints under axial loading are thus needed to facilitate the fatigue design.

This study aims to investigate the SCFs of HSS fabricated box X-joints under brace and chord axial loading. Four fabricated box X-joints with a nominal yield stress of 890 MPa were tested under brace axial compression. Strip strain gauges were used to obtain the SCFs of test specimens. Extensive FE simulations on the box X-joints under brace and chord axial loading were conducted. The effects of brace to chord width ratio, chord width to wall thickness ratio and brace to chord wall thickness ratio on the SCFs at typical hot spot locations were examined. The obtained test and FE results were used to assess the applicability of CIDECT SCF formulae and to propose suitable SCF equations for the box X-joints.

2. Hot spot stress method

The stiffness around the brace-chord intersection of tubular joints is not uniform. This results in non-uniform stress distribution. The hot spot stress is the maximum geometrical stress occurring at the intersection where the fracture usually initiates. The hot spot stress method determines the high-cycle fatigue resistance of tubular joints using the S_{rhs}-N_f curves where the S_{rhs} is the hot spot stress range and N_f is the cycle number to fatigue failure. It is noted that if $N_f \geq 10^4$, it is generally categorised as high-cycle fatigue failure. The hot spot stress method directly considers the effect of the uneven stress distribution at the brace-chord intersection and excludes the influence of local weld geometry (e.g. concave or convex weld profile) which can vary considerably in fabrication.

For the fatigue design of tubular joints, the internal forces in the chord and brace can be derived from structural analyses. It is convenient to calculate the corresponding nominal stress ranges in the member using the internal forces and sectional properties. The hot spot stress range can be obtained from tests and sophisticated FE simulations which are, however, not readily feasible for designers. The SCF is therefore employed as the multiplication factor on the nominal stress range to facilitate the determination of the hot spot stress range. The hot spot locations (i.e. locations of interest) where the stress concentration is pronounced are identified, along which the SCFs are determined. It is noted that the stress concentration

is mainly resulted from the geometric and stiffness discontinuities in the intersection region. Fig. 1 shows the hot spot locations specified in the CIDECT design guide No. 8 [4] for RHS T- and X-joints.

The SCFs at the hot spot locations can be derived from tests or FE analyses. The extrapolation region which is not affected by the local weld geometry is adopted to extrapolate the maximum stresses or strains at the weld toe (i.e. the hot spot stresses or hot spot strains) using those within the extrapolation zone. The linear and quadratic extrapolation methods are suggested for CHS and RHS joints, respectively [4]. This is because the gradients of stresses and strains at the hot spot locations of RHS joints are steep. Fig. 2 illustrates the CIDECT extrapolation region and extrapolation methods. The σ_{Max} is the maximum stress, ε_{Max} is the maximum strain, and t is the smaller wall thickness of the brace and chord. The strain concentration factor (SNCF) of CHS and RHS joints is defined as the ratio of the hot spot strain (ε_{Max}) to the nominal strain in the brace or chord. Strip strain gauges are usually used to derive the strain perpendicular to the weld toe and the SNCF because the stress measurement is not readily feasible in tests. Multiplication factors of 1.1 and 1.2 on the SNCFs are recommended to obtain the SCFs of RHS and CHS joints, respectively [4]. It is noted that the first measuring point is stipulated to be at least $0.4t$ with a minimum of 4 mm away from the weld toe.

The SCFs of RHS joints are mainly governed by the loading type and geometric parameters including the brace to chord width ratio (β), chord width to wall thickness ratio (2γ) and brace to chord wall thickness ratio (τ). The CIDECT SCF formulae for the typical hot spot locations (see lines A to E in Fig. 1) in RHS X- and T-joints under brace axial loading are as follows [4]:

$$\mathrm{SCF}_{\mathrm{C,ax,A}} = \mathrm{SCF}_{\mathrm{C,ax,E}} = \left(0.013 + 0.693\beta - 0.278\beta^2\right)(2\gamma)^{\left(0.790 + 1.898\beta - 2.109\beta^2\right)} \quad (1)$$

$$\mathrm{SCF}_{\mathrm{C,ax,B}} = \left(0.143 - 0.204\beta + 0.064\beta^2\right)(2\gamma)^{\left(1.377 + 1.715\beta - 1.103\beta^2\right)}\,\tau^{0.75} \quad (2)$$

$$\mathrm{SCF}_{\mathrm{C,ax,C}} = \left(0.077 - 0.129\beta + 0.061\beta^2 - 0.0006\gamma\right)(2\gamma)^{\left(1.565 + 1.874\beta - 1.028\beta^2\right)}\,\tau^{0.75} \quad (3)$$

$$\mathrm{SCF}_{\mathrm{C,ax,D}} = \left(0.208 - 0.387\beta + 0.209\beta^2\right)(2\gamma)^{\left(0.925 + 2.389\beta - 1.881\beta^2\right)}\,\tau^{0.75} \quad (4)$$

For RHS X- and T-joints with fillet welds at the brace-chord intersection, the SCFs on the brace side (i.e. $\mathrm{SCF}_{\mathrm{C,ax,A}}$ and $\mathrm{SCF}_{\mathrm{C,ax,E}}$) should be multiplied by a factor of 1.40. For X-joints with β=1.0, the $\mathrm{SCF}_{\mathrm{C,ax,C}}$ and $\mathrm{SCF}_{\mathrm{C,ax,D}}$ should be multiplied by factors of 0.65 and 0.50, respectively. The CIDECT SCF formulae for the lines A to E in RHS X- and T-joints subjected to chord axial loading are as follows [4]:

$$\mathrm{SCF}_{\mathrm{C,ch,A}} = \mathrm{SCF}_{\mathrm{C,ch,B}} = \mathrm{SCF}_{\mathrm{C,ch,E}} = 0 \text{ (negligible)} \quad (5)$$

$$\mathrm{SCF}_{\mathrm{C,ch,C}} = 0.725(2\gamma)^{0.248\beta}\,\tau^{0.19} \quad (6)$$

$$\mathrm{SCF}_{\mathrm{C,ch,D}} = 1.373(2\gamma)^{0.205\beta}\,\tau^{0.24} \quad (7)$$

A minimum SCF of 2.0 is suggested for all the hot spot locations and all loading conditions unless otherwise specified as negligible. This is because the hot spot stress which is determined along the limited fixed lines may underestimate the true hot spot stress if the direction of principal stress deviates from the fixed lines. Furthermore, the FE modelling is difficult for cases where β=1.0 and weld shapes have significant effects on SCFs, and crack initiation at the weld root can occur for low SCFs. The validity ranges of Eqs. (1-7) are $0.35\leq\beta\leq1.0$, $12.5\leq2\gamma\leq25.0$ and $0.25\leq\tau\leq1.0$. It should be noted that the CIDECT SCF formulae are originally proposed for normal strength steel hot-finished and cold-formed RHS X- and T-joints with round tube corners. The CIDECT S_{rhs}-N_{f} curves are only applicable for thick-walled RHS joints with tube wall thickness of 4 mm and larger which may be unconservative for RHS joints with smaller tube wall thickness [23]. The suitability of CIDECT SCF formulae for HSS fabricated box joints with sharp tube corners needs to be examined.

3. Experimental investigation

3.1. Test specimens

Tests were carried out on four fabricated box X-joints which were composed of built-up steel tubes. Fig. 3 illustrates the configuration and notations of the fabricated box X-joints. Full penetration butt weld at the tube corner was used to weld four steel plates into the box tube, and fillet weld at the brace-chord intersection was employed to assemble the tubes into the joint specimens. End plates were welded to the two brace ends in order to allow for applying uniform axial compression at the brace ends. Table 1 summarises the measured dimensions of the test specimens which are labelled in accordance with the nominal dimensions of brace and chord members. For example, the label of X-C120×6-B60×6 denotes the chord (C) having the nominal b_0=h_0=120 mm, nominal t_0=6 mm, and the brace (B) having the nominal b_1=h_1=60 mm, nominal t_1=6 mm. One parental HSS steel plate was used to fabricate the box tubes and the measured brace and chord wall thickness was 6.14 mm. The angle between the brace and chord members (θ) was 90°. The nominal lengths of the brace and chord were taken as L_1=3b_1 and L_0=6b_0, respectively, in order to avoid influences of brace and chord end conditions on the stress distribution at the brace-chord intersection [24].

A Q890 HSS plate with a nominal yield stress of 890 MPa which was manufactured by the quenching and tempering (QT) technique was used to fabricate the box tubes. The material properties of this steel plate

were reported by Lan et al. [25], and the measured elastic modulus (E) and yield stress (f_y) were 207 GPa and 907 MPa, respectively. The gas metal arc welding (GMAW) was employed to fabricate the box tubes and to assemble the joint specimens. The full penetration butt welds and fillet welds were designed in accordance with the requirements stipulated in AWS D1.1/D1.1M [26]. Table 1 summarises the measured dimensions of the reinforcement of the butt weld in the chord (i.e. b_w and h_w as shown in Fig. 3) and the weld leg size of the fillet weld (w). It should be noted that the reinforcement of the butt weld in the brace was trimmed off (i.e. b_w=h_w=0) to get flat surfaces for the strain measurement and to avoid the accumulation of the weld seams of the brace butt weld and the fillet weld. The typical values of f_y and f_u of the filler wire used for welding were 930 MPa and 980 MPa, respectively [27]. A robotic welding machine was employed to achieve a consistent and low heat input of 0.38 kJ/mm determined in line with the SSAB Welding Handbook [28], and the adopted values of current, voltage and welding speed for welding were 150A, 16V and 300 mm/min, respectively [25, 29]. Such low heat input used can alleviate the material softening in the heat affected zones and minimise the residual stresses resulted from welding for HSS [30-31].

3.2. Strain measurement

The nominal strain in the brace and the hot spot strain at the hot spot location (see Fig. 1) were measured to determine the SNCF of the test specimens. Fig. 4 shows the strain measurement in tests. Four single-element strain gauges were used for each test specimen in order to measure the nominal strain at the mid-length of the upper brace. The strain gauges were positioned near the four corners of the upper brace in order to eliminate any possible influences of local buckling of the brace. The average reading of the four strain gauges was taken as the nominal strain in the brace. The strain distribution in lines A to E was obtained by using five strip strain gauges for each specimen. The strain measurement was taken for only one corner of the intersection of the upper brace and the chord because of the geometric symmetry. Such strip strain gauges were composed of five uniaxial strain gauges on a 12 mm backing and could allow for the strain measurement at a 2 mm interval simultaneously. The strip strain gauges were placed adjacent to the weld toe, and the first measuring point was 2 mm away from the weld toe. This is to examine the effect of local weld toe geometry. The remaining four strain gauges of the strip strain gauge which were 4, 6, 8 and 10 mm away from the weld toe were positioned within the recommended CIDECT extrapolation region. It should be noted that the rusts on the surface where the strain measurement was taken were polished using sandpapers to ensure that the strain gauges were firmly attached to the test specimens.

3.3. Test set-up and procedure

The test set-up adopted for the test specimens is shown in Fig. 4. A servo-controlled hydraulic testing machine with maximum capacity of 1000 kN was used to apply the brace axial compression. The ends of the chord could freely translate and rotate. Base plates were fastened to the ball bearing and the actuator ram. The four vertical bolts were initially loosened and thus the ball bearing could rotate freely to self-adjust according to the flat profile of the brace end plate. A small preload of 4 kN was then applied by driving the specimens upwards using the actuator of the testing machine which was hidden below the floor. Therefore, any possible gaps between the brace end plate and the base plate could be eliminated. The vertical bolts were tightened afterwards to lock the position of the ball bearing. This is to avoid any rotations in the subsequent testing and to apply pure axial compression at the brace end. The testing was continued after preloading by driving the actuator ram upwards at a rate of 6 kN/min using the mode of load-control. Tests were paused for two minutes at predetermined load levels of 24, 36, 48, 60 and 72 kN to allow for stress relaxation and to consider the time lag of data acquisition device. It is noted that changes of the applied load at the brace end were negligible during the pauses. The applied loading and readings of strain gauges were recorded, and the test results at the predetermined load levels were employed to derive the SNCFs of test specimens. Displacement-control mode was used after reaching the maximum load level of 72 kN for the subsequent testing on the static strengths of the test specimens so that the testing could be continued in the post-ultimate range.

3.4. Test results

The CIDECT quadratic extrapolation method for RHS joints was adopted to calculate the hot spot strain at the weld toe for the fabricated box X-joints. This is because the nonlinear strain distribution against the distance from the weld toe was also observed for lines A to E. It is also noted that including the strains at the first measuring point of each strip strain gauge could lead to larger scatter for the quadratic extrapolation. This is possibly because the first measuring point which is only 2 mm away from the weld toe was affected by the local geometry of the fillet weld. The shape of the fillet weld was observed to be not uniform as shown in Fig. 4. Thus, only the other four strains which were obtained within the CIDECT extrapolation region (see Fig. 2) were used for the quadratic extrapolation. The obtained nominal strains and hot spot strains were observed to linearly increase with increasing brace loading. The differences between the calculated SNCFs at different predetermined load levels for each hot spot location are negligible because the stress and strain within the test specimens were in the elastic range. The mean SNCFs at various predetermined load levels were used in this study. The derived SNCFs were multiplied

by a factor of 1.1 to obtain the SCFs for the test specimens, in line with the CIDECT design guide No. 8 [4]. Table 2 summarises the SCFs obtained from tests.

The SCFs of lines A to E in the test specimens are shown in Fig. 5. It is observed that the highest SCF occurs in line B where the geometric discontinuity caused by the sharp corners of the brace and chord is pronounced. It is also noteworthy that β=0.5, τ=1.0 and 2γ ratio ranged from 19.9 to 49.1 for the four test specimens. The corresponding SCF dramatically increases (e.g. from 11.47 to 61.84 for line B) with increasing 2γ ratio. Therefore, slender chord cross-sections with large 2γ ratios are not recommended in order to avoid pronounced stress concentration at the brace-chord intersection. It is noted that higher SCFs generally lead to lower fatigue resistance of tubular joints. This is also in line with the CIDECT design philosophy which limits the range of 2γ ratio up to 25 (see Section 2). The SCFs predicted by the CIDECT SCF formulae ($SCF_{C,ax}$) were compared with the SCFs obtained from tests ($SCF_{Test,ax}$) as shown in Table 3. Fig. 5 further illustrates the corresponding comparison for lines A to E. The maximum $SCF_{C,ax}$ predicted is also in line B which coincides with the test results. The mean values of the $SCF_{Test,ax}/SCF_{C,ax}$ ratio are 0.59, 0.60, 0.59, 0.49 and 0.19 for lines A to E, respectively, with corresponding COVs of 0.141, 0.100, 0.164, 0.154 and 0.221. It is shown that the CIDECT SCF formulae over-predict the SCFs of lines A to E and are on the conservative side. The current CIDECT SCF formulae are thus not suitable for the fabricated box X-joints. This could be attributed to that the CIDECT SCF formulae are empirical in nature and are proposed for cold-formed and hot-finished RHS joints with round tube corners.

4. Finite element investigation

4.1. Finite element model

FE simulations on the fabricated box X-joints was conducted using ABAQUS version 6.13 [32] in order to cover a wide range of joint parameters. A FE model was constructed and validated against the test results summarised in Section 3.4 of this paper. The measured dimensions summarised in Table 1 were adopted. Fig. 6 depicts the developed FE model for the validation study. Quadratic solid elements in ABAQUS were employed. The brace and chord in blue colour (see Fig. 6) were modelled by the twenty-node hexahedron solid element (C3D20R). The ten-node tetrahedron solid element (C3D10) was adopted to simulate the fillet weld (in orange colour). The six-node linear wedge solid element (C3D15) was used to model the reinforcement of the butt weld in the chord (in green colour). The mesh sizes for the FE model were carefully determined by a mesh convergence study. A suitable mesh size of 6 mm was adopted for the brace, chord and reinforcement of the chord butt weld, and the mesh size used for the

fillet weld was 3 mm. Four layers of the C3D20R element through the brace and chord wall thickness were employed for $b_0/t_0<20$ and $b_1/t_1<20$ while two element layers were used for $b_0/t_0\geq20$ and $b_1/t_1\geq20$ [6, 21]. Further reducing the mesh sizes and increasing the mesh layers result in the changes of the predicted SCFs within 2% of the test SCFs.

The measured elastic modulus (E) of 207 GPa and the Poisson's ratio (v) of 0.3 were adopted to perform the linear-elastic FE simulations on the box X-joints. The material and geometric nonlinearities were not considered and thus the obtained SCFs were not affected by the load levels [12]. The degrees of freedom of all nodes at the brace end were coupled to a concentric reference point by using rigid body constraints. All degrees of freedom of the brace reference point were restricted except for the brace axial translation. The chord ends could freely translate and rotate. The "tie" function in the ABAQUS was used in order to tie the reinforcement of the chord butt weld to the chord side wall and to tie the fillet weld to the brace and chord flange. Axial compression was applied in increments to the brace reference point. It should be noted that the residual stresses in the fabricated box X-joints were not simulated because the lower heat input used for welding could lead to small residual stresses. The quadratic extrapolation method was used to extrapolate the hot spot strain using the four strains within the CIDECT extrapolation region. The SNCF defined as the ratio of the hot spot strain to the nominal strain in the brace was multiplied by a factor of 1.1 to derive the SCF.

Fig. 5 shows the comparison of the SCFs obtained from the tests ($SCF_{Test,ax}$) with those predicted by the FE analyses ($SCF_{FE,ax}$). Table 3 summarises the $SCF_{Test,ax}/SCF_{FE,ax}$ ratio for the test specimens. The mean values of the $SCF_{Test,ax}/SCF_{FE,ax}$ ratio are 0.95, 0.88, 0.94, 0.87 and 0.98 for lines A to E, respectively, with corresponding COVs of 0.106, 0.078, 0.073, 0.078 and 0.064. The constructed FE model, in general, slightly over-predicts the test SCFs which is on the conservative side. Such discrepancy could be attributed to the residual stresses which were not modelled in the FE model and the inevitable scatter of test results caused during the fabrication and measurement processes. Nevertheless, it can be concluded that the FE model produces reasonably accurate SCF predictions when compared with the test results. Therefore, the developed FE model will be used for the subsequent FE parametric study.

4.2. Parametric study

A parametric study on totally 112 fabricated box X-joints was conducted including 56 joint configurations and two loading cases of brace axial loading and chord axial loading. The FE model developed in Section 4.1 of this paper was adopted. The chord width and chord depth were set to be 200 mm. The parametric

study covers a wide range of geometric parameters i.e. β=0.35, 0.50, 0.65, 0.80, 2γ=12.5, 16.0, 20.0, 25.0, and τ=0.25, 0.50, 0.75, 1.00. The angle between the brace and chord members (θ) was set to be 90°. The brace length (L_1) was set to be $3b_1$ and the chord length (L_0) was taken as $6b_0$. Tables 4-5 summarise the key joint parameters for each FE specimen.

The chord wall thickness ranged from 8 to 16 mm and the brace wall thickness varied from 2 to 16 mm in the parametric study. The full penetration butt weld is commonly adopted to assemble tubes with wall thickness of 8 mm and larger in practice to achieve economical weld design; otherwise, the required weld leg size would be relatively large if the fillet weld is used. Therefore, the weld assembling the brace and chord into the joint specimen was modelled in line with the minimum requirements for the butt weld stipulated by AWS D1.1/D1.1M [26]. Fig. 7 illustrates the profile of the butt weld adopted for the parametric study which was also used by Daneshvar et al. [7] and Tong et al. [33-34]. The portion of the butt weld in orange (see Fig. 7) was modelled using the tetrahedron solid element (C3D10) and was tied to the brace and chord flange using the "tie" function in ABAQUS. The brace and chord members were simulated by the hexahedron solid element (C3D20R).

The reinforcement of the butt weld in the chord which is denoted in green (see Fig. 6) was not modelled for the parametric study. This is because such reinforcement could be trimmed off in the finished products of such box tubes in practice for aesthetic appearance. It is noted that the reinforcement of the butt weld in box tubes which were used to fabricate the box T-joints was also trimmed off [19-20]. Furthermore, the reinforcement can alleviate the stress concentration and lower the SCFs because it can mitigate the geometric discontinuity at the chord corner. The SCFs derived from the FE model which excludes the reinforcement modelling could be higher. Such approach is therefore on the conservative side. It is also noted that the dimensions of the reinforcement could vary considerably in practice. The reinforcement of the brace butt weld was also not modelled.

Similar to the FE model developed in Section 4.1, suitable mesh sizes were employed, i.e. 6 mm for the brace and chord members, and $t_1/4$ for the portion of the butt weld in orange (see Fig. 7). The boundary conditions used for the validation study in Section 4.1 of this paper were adopted for the loading cases of brace and chord axial loading herein. All degrees of freedom at the two brace ends were restricted except for the brace axial translation, and the degrees of freedom at the two chord ends were not restrained. Only axial compression was applied at the two brace ends for the loading case of brace axial loading. Similarly, only axial compressive forces were applied at the two chord ends for the loading case of chord axial loading. The applied maximum forces at the brace and chord ends was predetermined so that the

corresponding maximum nominal stress in the brace and chord members was 10 MPa. It should be noted that there are, to the best knowledge of the authors, no test results of the box X-joints under chord axial loading in the literature. The FE modelling methodology which has been validated against the test results for the loading case of brace axial loading was thus adopted for the loading case of chord axial loading. The subsequent analyses described in Section 4.3 and proposed SCF equations summarised in Section 5 are based on the FE results obtained in this section.

4.3. FE results

4.3.1. General

The FE stresses of lines A to E in the parametric study also exhibited nonlinear stress distributions against the distance from the weld toe. Therefore, the CIDECT quadratic extrapolation was adopted to obtain the hot spot stresses at the weld toe using the stresses within the CIDECT extrapolation region. The applied brace and chord loads divided by the cross-section areas of the brace and chord, respectively, were taken as the nominal stresses. The FE SCFs for brace axial loading ($SCF_{FE,ax}$) and chord axial loading ($SCF_{FE,ch}$) were calculated as the ratio of the hot spot stress to the nominal stress. Tables 4-5 tabulate the $SCF_{FE,ax}$ and $SCF_{FE,ch}$ obtained from the parametric study.

4.3.2. Brace axial loading

The SCFs of line E for the loading case of brace axial loading are not listed in Table 4. This is because the SCF values of line A are consistently higher than those of line E for the brace member and thus line E is not a location of interest. This could be attributed to that line A is closer to the sharp chord corner and therefore the geometric discontinuity of the adjacent region is more pronounced. The stress concentration which is mainly caused by the geometric and stiffness discontinuities is more significant for line A. The subsequent analyses and the proposed SCF equations exclude line E. Fig. 8 illustrates the representative SCF distributions of lines A to D for the loading case of brace axial loading. The SCFs of line B are generally higher than those of lines C and D for the chord member because the geometric discontinuity in line B where is closer to the sharp chord corner is more pronounced.

The geometric parameters have significant influences on the SCFs of the box X-joints under brace axial loading. The SCFs generally increase and then decrease with increasing β ratio, and the highest SCFs typically occur for medium β ratios (i.e. β=0.50 and 0.65). It is noted that the axial stiffness of the brace

wall is usually higher than the out-of-plane bending stiffness of the chord face adjacent to the intersection region. The stiffness difference between the two which governs the SCFs increases with increasing β ratio and then decreases when β ratio approaches to unity. This could be attributed to that the brace-chord intersection is closer to the fairly rigid chord corners which can substantially enhance the out-of-bending stiffness of the chord face. The stiffness difference and the corresponding SCFs are thus smaller when β ratio approaches to unity. It should be noted that the SCFs of line C for β=0.35 and 0.50 are close and such trend is also observed for line D (see Figs. 8(c-d)). The effect on SCFs could be approximated by a parabolic function of β ratio.

The SCFs are also shown to increase with increasing 2γ and τ ratios. This can also be explained by that the out-of-plane bending stiffness of the chord face decreases with increasing 2γ ratio and the axial stiffness of the brace wall increases with increasing τ ratio. Thus, the stiffness difference between the two and SCFs increase for higher 2γ and τ ratios. The effects on SCFs could be represented by exponential functions of 2γ and τ ratios. Similar effects of β, 2γ and τ ratios on SCFs are also observed for hot-finished and cold-formed RHS X-joints under brace axial loading [4].

The SCFs calculated from the CIDECT SCF formulae for the loading case of brace axial loading ($SCF_{C,ax}$) were compared with those obtained from the FE parametric study ($SCF_{FE,ax}$) as depicted in Fig. 9. Table 4 shows that the mean values of $SCF_{FE,ax}/SCF_{C,ax}$ for lines A, B, C and D are 0.91, 1.16, 0.78 and 1.16, respectively, and the corresponding COVs are 0.121, 0.145, 0.217 and 0.141. This indicates that the CIDECT SCF predictions are, in general, not accurate for the fabricated box X-joints, and thus more suitable SCF equations are needed.

It should be noted that the CIDECT SCF equations (Eqs. (1-7)) are originally proposed by van Wingerde [35], which were derived from regression analyses of numerical results obtained using a FE model with butt welds and a ratio of chord corner radius (r_0) to the chord wall thickness (t_0) of 2.0. The influence of corner radius on the SCFs is shown to be significant; however, the corresponding correction function of corner radius is not proposed and used, aiming to achieve a balance of simplicity and accuracy for the SCF equations [35]. It is evident that the fabricated box X-joints with sharp tube corners (i.e., r_0/t_0=0) are beyond the validity ranges of the CIDECT SCF equations. It would be better to treat the fabricated box X-joints and cold-formed/hot-finished counterparts as two different joint configurations and adopt corresponding SCF equations for each joint configuration, considering the pronounced effect of the corner radius.

4.3.3. Chord axial loading

The SCFs of lines A, B, C and E for the loading case of chord axial loading are not tabulated in Table 5 because the corresponding maximum SCFs were 0.45, 0.26, 1.22 and 0.34 and thus these lines were not locations of interest. The subsequent analyses and the proposed SCF equation will be based on line D only. Fig. 10 shows the representative SCF distributions of line D. The SCFs increase with increasing β and τ ratios and with decreasing 2γ ratio; however, the effect of 2γ ratio is relatively insignificant. This could be attributed to the aforementioned geometric discontinuity at the brace-chord intersection. The line D is closer to the sharp chord corner for larger β ratio and the geometric discontinuity is more pronounced which results in higher SCFs. Larger 2γ ratio and smaller τ ratio (i.e. thinner tube walls of the brace and chord) mitigate the stress concentration and lower the SCFs in line D. The effects on SCFs could be represented by a linear function of β ratio and exponential functions of 2γ and τ ratios. Such effects of β, 2γ and τ ratios on the SCFs are also observed for hot-finished and cold-formed RHS X-joints under chord axial loading [4].

Fig. 11 illustrates the comparison of the CIDECT SCFs ($SCF_{C,ch}$) of line D with the corresponding FE SCFs ($SCF_{FE,ch}$) for the loading case of chord axial loading. Table 5 shows that the mean value of the $SCF_{FE,ch}/SCF_{C,ch}$ ratio for line D is 1.02 with corresponding COV of 0.102. The CIDECT SCF predictions are generally scattered for the box X-joints, and therefore a more appropriate SCF equation is needed.

5. Proposed SCF equations

The CIDECT SCF formulae for cold-formed and hot-finished RHS joints under axial loading are mainly based on the research work conducted by van Wingerde et al. [35-36], and the adopted general format of the SCF equations is as follows:

$$\mathrm{SCF} = \left(a + b\beta + c\beta^2 + d\gamma\right)\left(2\gamma\right)^{\left(e + f\beta + g\beta^2\right)} \tau^h \tag{8}$$

where the coefficients of *a*, *b*, *c*, *d*, *e*, *f*, *g* and *h* vary with locations of interest and loading types. Multiple regression analyses using the least squares method are typically employed to determine these coefficients. For chord axial loading, the SCF formula is simplified as follows:

$$\mathrm{SCF} = a\left(2\gamma\right)^{f\beta} \tau^h \tag{9}$$

The analyses described in Section 4.3 of this paper show that the effect of geometric parameters (i.e. β, 2γ and τ ratios) on the SCFs for the loading case of brace axial loading could be approximated by a parabolic

function of β ratio and exponential functions of 2γ and τ ratios. The effects of the geometric parameters on the SCFs for the loading case of chord axial loading could be represented by a linear function of β ratio and exponential functions of 2γ and τ ratios. This thus demonstrates that the CIDECT general formats of the SCF equations (Eqs. (8-9)) are applicable for the fabricated box X-joints and are employed herein.

Regression analyses of the SCFs obtained in Section 4.2 of this paper were conducted. The SCF formulae for the box X-joints under brace axial loading were proposed as follows:

$$SCF_{P,ax,A} = \left(-0.083 + 0.838\beta - 0.240\beta^2\right)(2\gamma)^{\left(1.390 - 0.241\beta - 0.367\beta^2\right)} \tau^{0.06} \quad (10)$$

$$SCF_{P,ax,B} = \left(1.322 - 3.039\beta + 1.773\beta^2\right)(2\gamma)^{\left(0.762 + 1.352\beta + 0.284\beta^2\right)} \tau^{0.78} \quad (11)$$

$$SCF_{P,ax,C} = \left(0.069 + 1.223\beta - 1.857\beta^2 + 0.034\gamma\right)(2\gamma)^{\left(0.938 + 0.628\beta - 0.534\beta^2\right)} \tau^{0.88} \quad (12)$$

$$SCF_{P,ax,D} = \left(0.153 - 0.134\beta - 0.014\beta^2\right)(2\gamma)^{\left(1.196 + 1.154\beta - 0.831\beta^2\right)} \tau^{0.50} \quad (13)$$

It is noted that line E is not location of interest as the SCFs of line E are lower than those of line A.

The proposed SCF equations for the box X-joints under chord axial loading are as follows:

$$SCF_{P,ch,A} = SCF_{P,ch,B} = SCF_{P,ch,C} = SCF_{P,ch,E} = 0 \text{ (negligible)} \quad (14)$$

$$SCF_{P,ch,D} = 1.391(2\gamma)^{0.152\beta} \tau^{0.10} \quad (15)$$

A minimum SCF of 2.0 is suggested for all the hot spot locations and all loading conditions unless otherwise specified as negligible, in accordance with the CIDECT design guide No. 8 [4]. The validity ranges of Eqs. (10-15) are $0.35 \le \beta \le 0.80$, $12.5 \le 2\gamma \le 25.0$ and $0.25 \le \tau \le 1.0$.

Figs. 12-13 illustrate the comparison of the SCFs calculated from the proposed SCF formulae ($SCF_{P,ax}$ and $SCF_{P,ch}$) with those obtained from the parametric study ($SCF_{FE,ax}$ and $SCF_{FE,ch}$). The results of corresponding statistical analyses are summarised in Tables 4-5. The mean values of the $SCF_{FE,ax}/SCF_{P,ax}$ ratio for lines A, B, C and D are 1.00, 1.00, 0.99 and 1.00, respectively, with corresponding COV of 0.074, 0.080, 0.069 and 0.095. The mean value of $SCF_{FE,ch}/SCF_{P,ch}$ for line D is 1.00 with corresponding COV of 0.061. It is shown that the proposed SCF equations can provide more accurate and consistent SCF predictions for the box X-joints when compared with the CIDECT SCF formulae.

It should be noted that the proposed SCF equations can also be applicable for normal strength steel fabricated box X-joints. This is because the SCFs are mainly governed by the joint configurations, loading types, joint geometric parameters and elastic material properties of steel. The elastic modulus and

454 the Poisson's ratio of normal strength steel and HSS are almost the same. Furthermore, the evaluation of
455 the applicability of the CIDECT fatigue design rules for HSS fabricated box X-joints under axial loading
456 consists of two vital parts, i.e. the suitability of the CIDECT SCF equations and S_{rhs}-N_f curves. The first
457 issue was addressed in this study and more tests on the fatigue resistances of HSS fabricated box X-joints
458 are needed in order to assess the appropriateness of the CIDECT S_{rhs}-N_f curves.
459
460 **6. Conclusions**
461
462 The stress concentration factor (SCF) is crucial for the hot spot stress method, which is widely used to
463 determine the high-cycle fatigue resistance of tubular joints. The sharp tube corners in high strength steel
464 (HSS) fabricated box X-joints can alter the stress concentration and affect the SCFs. Thus, tests and FE
465 simulations on the SCFs of HSS fabricated box X-joints under brace and chord axial loading were
466 conducted. Four fabricated box X-joints with a nominal yield stress of 890 MPa were tested under brace
467 axial compression. A finite element (FE) model was developed which has been validated against the
468 obtained test results. An extensive parametric study using the validated FE model was conducted on the
469 box X-joints subjected to brace and chord axial loading. A wide range of brace to chord width ratio (β),
470 chord width to wall thickness ratio (2γ) and brace to chord wall thickness ratio (τ) were covered. The
471 CIDECT SCF formulae were assessed against the obtained test and FE results. It is shown that the SCFs
472 of the box X-joints under brace axial loading generally increase and then decrease with increasing β ratio,
473 and are higher for larger 2γ and τ ratios. The SCFs of the box X-joints under chord axial loading, in
474 general, increase with increasing β and τ ratios, and the effect of 2γ ratio on the SCFs is relatively
475 insignificant. The CIDECT SCF formulae are not suitable for the box X-joints. Hence, SCF equations
476 which can provide more accurate and consistent SCF predictions are proposed for the box X-joints in this
477 study.
478

References

[1] X.Y. Lan, T.M. Chan, Recent research advances of high strength steel welded hollow section joints, Struct. 17 (2019) 58-65.

[2] International Institute of Welding (IIW), Recommended fatigue design procedure for hollow section joints. Part 1-Hot spot stress method for nodal joints, IIW Subcommission XV-E, IIW Doc. XV-582-85, IIW Assembly, Strasbourg, France, 1985.

[3] International Organization for Standardization (ISO), Fatigue-design procedure for welded hollow-section joints-recommendations, ISO 14347:2008, ISO, Geneva, Switzerland, 2008.

[4] X.L. Zhao, S. Herion, J.A. Packer, R.S. Puthli, G. Sedlacek, J. Wardenier, K. Weynand, A.M. van Wingerde, N.F. Yeomans, Design guide for circular and rectangular hollow section welded joints under fatigue loading, CIDECT Design Guide No. 8, CIDECT, Germany, 2001.

[5] F. Wang, O. Zhao, B. Young, Testing and numerical modelling of S960 ultra-high strength steel angle and channel section stub columns, Eng. Struct. 204 (2020) 109902.

[6] R. Feng, B. Young, Stress concentration factors of cold-formed stainless steel tubular X-joints, J. Constr. Steel Res. 91 (2013) 26-41.

[7] S. Daneshvar, M. Sun, K. Karimi, Galvanized RHS X-Connections. I: Effects of vent and drain holes on SCFs, J. Constr. Steel Res. 167 (2020) 105854.

[8] S. Daneshvar, M. Sun, Stress concentration factors of RHS T-connections with galvanizing holes under in-plane bending, J. Constr. Steel Res. 169 (2020) 106039.

[9] F.N. Matti, F.R. Mashiri, Experimental and numerical studies on SCFs of SHS T-joints subjected to static out-of-plane bending, Thin Wall. Struct. 146 (2020) 106453.

[10] F.N. Matti, F.R. Mashiri, Parametric study on SCFs of SHS-SHS T-joint connections under out-of-plane brace bending, Eng. Struct. 221 (2020) 111032.

[11] C. Li, F. Huang, Y. Lou, B. Cheng, Stress concentration factors of bird-beak SHS X-joints under brace axial forces. J. Constr. Steel Res. 150 (2018) 87-98.

[12] B. Cheng, F. Huang, C. Li, Y. Duan, X.L. Zhao, Hot spot stress and fatigue behavior of bird-beak SHS X-joints subjected to brace in-plane bending, Thin Wall. Struct. 150 (2020) 106701.

[13] Y. Chen, J. Wan, K. Hu, J. Yang, X. Chen, Stress concentration factors of circular chord and square braces K-joints under axial loading, Thin Wall. Struct. 113 (2017) 287-298.

[14] R. Feng, C. Tang, K. Roy, Z. Chen, B. Chen, J.B. Lim, An experimental study on stress concentration factors of stainless steel hybrid tubular K-joints, Thin Wall. Struct. 157 (2020) 107064.

[15] G. Xu, L. Tong, X.L. Zhao, H. Zhou, F. Xu, Numerical analysis and formulae for SCF reduction coefficients of CFRP-strengthened CHS gap K-joints, Eng. Struct. 210 (2020) 110369.

[16] H. Ahmadi, A. Kouhi, Stress concentration factors of multi-planar tubular XT-joints subjected to out-of-plane bending moments, Appl. Ocean Res. 96 (2020) 102058.

[17] Y. Jiang, K. Yuan, H. Cui, Prediction of stress concentration factor distribution for multi-planar tubular DT-joints under axial loads, Mar. Struct. 61 (2018) 434-451.
[18] S. Bao, W. Wang, X. Li, H. Zhao, Hot-spot stress caused by out-of-plane bending moments of three-planar tubular Y-joints, Appl. Ocean Res. 100 (2020) 102179.
[19] J. Jiang, C.K. Lee, S.P. Chiew, Residual stress and stress concentration effect of high strength steel built-up box T-joints, J. Constr. Steel Res. 105 (2015) 164-173.
[20] S.P. Chiew, M.S. Zhao, C.K. Lee, Fatigue performance of high strength steel built-up box T-joints, J. Constr. Steel Res. 106 (2015) 296-310.
[21] L. Jiang, Y. Liu, A. Fam, Stress concentration factors in joints of square hollow section (SHS) brace and concrete-filled SHS chord under axial tension in brace, Thin Wall. Struct. 132 (2018) 79-92.
[22] L. Jiang, Y. Liu, J. Liu, B. Liu, Experimental and numerical analysis of the stress concentration factor for concrete-filled square hollow section Y-joints, Adv. Struct. Eng. 23(5) (2020) 869-883.
[23] X. L. Zhao, L.W. Tong, New development in steel tubular joints, Adv. Struct. Eng. 14(4) (2011) 699-715.
[24] X.Y. Lan, Y. Huang, Structural design of cold-formed stainless steel tubular X- and T-joints at elevated temperatures, Thin Wall. Struct. 108 (2016) 270-279.
[25] X.Y. Lan, T.M. Chan, B. Young, Structural behaviour and design of high strength steel RHS X-joints, Eng. Struct. 200 (2019) 109494.
[26] AWS. Structural welding code-steel. AWS D1.1/D1.1M: 2010, United States.
[27] X.Y. Lan, T.M. Chan, B. Young, Testing, finite element analysis and design of high strength steel RHS T-joints, Eng. Struct. 227 (2021) 111184.
[28] SSAB. Welding handbook-A guide to better welding of Hardox and Weldox, 2009, Sweden.
[29] M. Pandey, B. Young, Tests of cold-formed high strength steel tubular T-joints, Thin Wall. Struct. 143 (2019) 106200.
[30] X.Y. Lan, T.M. Chan, B. Young, Experimental study on the behaviour and strength of high strength steel CHS T- and X-joints, Eng. Struct. 206 (2020) 110182.
[31] X.Y. Lan, T.M. Chan, B. Young, Structural behaviour and design of high strength steel CHS T-joints, Thin Wall. Struct. 159 (2021) 107215.
[32] Abaqus/Standard. Version 6.13-1. USA: K. a. S. Hibbit; 2013.
[33] L.W. Tong, G.W. Xu, Y.Q. Liu, D.Q. Yan, X.L. Zhao, Finite element analysis and formulae for stress concentration factors of diamond bird-beak SHS T-joints, Thin Wall. Struct. 86 (2015) 108-120.
[34] L.W. Tong, G.W. Xu, D.L. Yang, F.R. Mashiri, X.L. Zhao, Stress concentration factors in CHS-CFSHS T-joints: experiments, FE Anal. Formulae. Eng. Struct. 151 (2017) 406-421.
[35] A.M. van Wingerde, The fatigue behaviour of T- and X-joints made of square hollow sections. Heron, 1992, 37(2), 1-180.
[36] A.M. van Wingerde, J.A. Packer, J. Wardenier, SCF formulae for fatigue design of K-connections between square hollow sections, J. Constr. Steel Res. 43 (1997) 87-118.

Table 1

Measured dimensions of high strength steel fabricated box X-joints.

Specimen	b_0 (mm)	h_0 (mm)	L_0 (mm)	b_1 (mm)	h_1 (mm)	L_1 (mm)	b_w (mm)	h_w (mm)	w (mm)
X-C120×6-B60×6	122.1	123.3	718	61.3	62.3	171	15.1	1.8	8.2
X-C180×6-B90×6	181.9	182.4	1080	91.1	92.0	260	15.3	1.9	7.1
X-C240×6-B120×6	240.3	242.5	1441	120.4	121.4	351	16.0	2.2	7.2
X-C300×6-B150×6	301.7	301.7	1801	151.3	151.6	439	15.3	1.7	6.7

Table 2

SCFs of fabricated box X-joint test specimens.

Specimen	β	2γ	τ	$SCF_{Test,ax}$				
				A	B	C	D	E
X-C120×6-B60×6	0.5	19.9	1.0	7.34	11.47	8.30	3.47	2.00
X-C180×6-B90×6	0.5	29.6	1.0	15.66	28.81	22.97	9.56	5.66
X-C240×6-B120×6	0.5	39.1	1.0	23.28	47.50	36.30	14.22	6.45
X-C300×6-B150×6	0.5	49.1	1.0	26.28	61.84	56.82	21.73	9.20

Table 3

Comparison of CIDECT and FE SCFs with those of fabricated box X-joint test specimens.

Specimen	β	2γ	τ	$SCF_{Test,ax}/SCF_{C,ax}$					$SCF_{Test,ax}/SCF_{FE,ax}$				
				A	B	C	D	E	A	B	C	D	E
X-C120×6-B60×6	0.5	19.9	1.0	0.48	0.58	0.46	0.37	0.13	0.90	0.80	0.86	0.86	0.96
X-C180×6-B90×6	0.5	29.6	1.0	0.63	0.66	0.60	0.53	0.23	1.02	0.92	0.97	0.96	1.06
X-C240×6-B120×6	0.5	39.1	1.0	0.67	0.63	0.60	0.50	0.19	1.04	0.95	1.01	0.84	0.99
X-C300×6-B150×6	0.5	49.1	1.0	0.57	0.53	0.70	0.53	0.20	0.83	0.85	0.91	0.81	0.91
Mean				0.59	0.60	0.59	0.49	0.19	0.95	0.88	0.94	0.87	0.98
COV				0.141	0.100	0.164	0.154	0.221	0.106	0.078	0.073	0.078	0.064

Table 4

FE results of 56 fabricated box X-joints under brace axial loading.

Joint no.	β	2γ	τ	$SCF_{FE,ax}$				$SCF_{FE,ax}/SCF_{C,ax}$				$SCF_{FE,ax}/SCF_{P,ax}$			
				A	B	C	D	A	B	C	D	A	B	C	D
1	0.35	12.5	0.25	4.15	3.70	2.11	2.15	0.91	1.26	0.85	1.30	1.03	0.93	0.94	0.94
2	0.35	12.5	0.50	4.34	6.90	4.25	3.65	0.96	1.39	1.01	1.31	1.04	1.01	1.03	1.12
3	0.35	12.5	0.75	4.05	9.17	5.84	4.33	0.89	1.37	1.03	1.15	0.94	0.98	0.99	1.09
4	0.35	12.5	1.00	3.67	10.86	7.33	4.51	0.81	1.30	1.04	0.96	0.84	0.92	0.96	0.98
5	0.35	16.0	0.25	5.67	4.68	2.98	2.82	0.93	1.01	0.73	1.17	1.03	0.86	0.90	0.85
6	0.35	16.0	0.50	6.19	9.25	6.09	4.93	1.01	1.19	0.89	1.21	1.08	0.99	1.00	1.05
7	0.35	16.0	0.75	5.72	12.25	8.70	5.85	0.94	1.16	0.94	1.06	0.98	0.95	1.00	1.02
8	0.35	16.0	1.00	5.18	14.87	10.76	6.13	0.85	1.13	0.94	0.90	0.87	0.92	0.96	0.92
9	0.35	20.0	0.25	7.42	6.78	4.41	3.99	0.93	0.97	0.70	1.17	1.02	0.94	0.93	0.86
10	0.35	20.0	0.50	8.57	13.30	8.96	7.19	1.08	1.13	0.85	1.26	1.13	1.07	1.03	1.10
11	0.35	20.0	0.75	7.81	18.20	12.93	8.56	0.98	1.14	0.91	1.10	1.01	1.07	1.04	1.07
12	0.35	20.0	1.00	7.06	20.93	16.17	8.89	0.89	1.06	0.91	0.92	0.89	0.98	1.01	0.96
13	0.35	25.0	0.25	9.36	8.53	6.00	5.41	0.90	0.81	0.63	1.13	0.97	0.89	0.87	0.83
14	0.35	25.0	0.50	11.51	16.92	12.50	9.62	1.11	0.95	0.78	1.19	1.15	1.02	0.98	1.05
15	0.35	25.0	0.75	10.52	23.36	18.05	11.72	1.01	0.97	0.83	1.07	1.02	1.03	0.99	1.04
16	0.35	25.0	1.00	9.44	28.81	23.05	12.56	0.91	0.96	0.85	0.93	0.90	1.02	0.99	0.97
17	0.50	12.5	0.25	4.96	3.78	1.95	2.03	0.80	1.33	0.79	1.33	1.00	1.00	0.91	0.94
18	0.50	12.5	0.50	5.46	7.35	4.00	3.47	0.88	1.54	0.97	1.36	1.05	1.14	1.02	1.14
19	0.50	12.5	0.75	5.45	9.26	5.63	4.08	0.88	1.43	1.00	1.18	1.03	1.04	1.00	1.10
20	0.50	12.5	1.00	5.36	11.86	6.63	3.96	0.87	1.48	0.95	0.92	0.99	1.07	0.92	0.92
21	0.50	16.0	0.25	6.54	4.95	2.87	2.71	0.78	1.08	0.70	1.19	0.98	0.91	0.90	0.86
22	0.50	16.0	0.50	7.36	9.74	5.96	4.88	0.88	1.26	0.86	1.27	1.06	1.04	1.01	1.09
23	0.50	16.0	0.75	7.18	12.96	8.44	5.60	0.86	1.24	0.90	1.08	1.01	1.01	1.00	1.02
24	0.50	16.0	1.00	6.87	15.52	10.57	5.69	0.82	1.19	0.91	0.88	0.95	0.96	0.97	0.90
25	0.50	20.0	0.25	8.35	7.07	4.31	3.96	0.76	0.99	0.67	1.20	0.97	0.92	0.92	0.88
26	0.50	20.0	0.50	10.07	14.19	9.01	6.89	0.92	1.18	0.84	1.24	1.12	1.08	1.05	1.09
27	0.50	20.0	0.75	9.39	19.53	12.79	8.08	0.86	1.20	0.88	1.07	1.02	1.08	1.04	1.04
28	0.50	20.0	1.00	8.76	23.30	15.88	8.11	0.80	1.16	0.88	0.87	0.93	1.03	1.00	0.90
29	0.50	25.0	0.25	10.30	9.32	6.08	5.47	0.72	0.85	0.62	1.15	0.92	0.87	0.88	0.86
30	0.50	25.0	0.50	13.10	18.81	12.79	9.69	0.91	1.01	0.77	1.21	1.12	1.02	1.00	1.08
31	0.50	25.0	0.75	12.07	25.42	18.19	11.74	0.84	1.01	0.81	1.08	1.00	1.01	1.00	1.07
32	0.50	25.0	1.00	11.10	30.68	22.80	12.19	0.77	0.98	0.82	0.90	0.91	0.97	0.97	0.96
33	0.65	12.5	0.25	4.84	3.04	1.34	1.57	0.80	1.38	0.66	1.42	0.96	1.10	0.92	0.93
34	0.65	12.5	0.50	5.42	5.64	2.76	2.83	0.90	1.52	0.81	1.52	1.03	1.18	1.03	1.19
35	0.65	12.5	0.75	5.71	7.24	3.79	3.21	0.94	1.44	0.82	1.27	1.06	1.11	0.99	1.10

36	0.65	12.5	1.00	5.67	8.18	4.49	3.14	0.94	1.31	0.78	1.00	1.03	1.00	0.91	0.93
37	0.65	16.0	0.25	6.22	4.05	2.11	2.13	0.78	1.11	0.63	1.26	0.94	0.95	0.91	0.85
38	0.65	16.0	0.50	7.52	8.10	4.42	3.83	0.94	1.32	0.78	1.35	1.10	1.10	1.04	1.08
39	0.65	16.0	0.75	7.24	10.65	6.18	4.39	0.91	1.28	0.81	1.14	1.03	1.06	1.01	1.01
40	0.65	16.0	1.00	7.15	12.42	7.43	4.35	0.89	1.21	0.78	0.91	1.00	0.98	0.95	0.87
41	0.65	20.0	0.25	7.73	5.89	3.38	3.24	0.75	1.03	0.65	1.32	0.92	0.93	0.95	0.91
42	0.65	20.0	0.50	9.79	11.90	7.04	5.74	0.95	1.24	0.81	1.39	1.12	1.09	1.08	1.14
43	0.65	20.0	0.75	9.04	16.08	9.82	6.69	0.88	1.23	0.83	1.20	1.01	1.08	1.05	1.08
44	0.65	20.0	1.00	8.76	18.43	11.79	6.56	0.85	1.14	0.80	0.95	0.96	0.99	0.98	0.92
45	0.65	25.0	0.25	9.49	8.02	4.86	4.44	0.72	0.89	0.63	1.25	0.89	0.85	0.89	0.87
46	0.65	25.0	0.50	12.27	16.42	10.27	7.99	0.93	1.09	0.79	1.33	1.10	1.02	1.02	1.11
47	0.65	25.0	0.75	12.26	22.89	14.52	9.18	0.92	1.12	0.82	1.13	1.08	1.03	1.01	1.04
48	0.65	25.0	1.00	10.78	26.60	17.83	9.55	0.81	1.05	0.81	0.95	0.93	0.96	0.96	0.94
49	0.80	12.5	0.25	3.99	1.28	0.36	0.96	0.91	1.00	0.26	1.37	0.88	0.89	1.06	0.95
50	0.80	12.5	0.50	4.86	2.10	0.65	1.60	1.11	0.98	0.28	1.35	1.03	0.85	1.05	1.11
51	0.80	12.5	1.00	5.09	3.79	1.13	2.10	1.16	1.05	0.29	1.06	1.03	0.89	0.99	1.03
52	0.80	20.0	0.25	5.93	3.81	1.86	1.91	0.86	1.14	0.57	1.26	0.83	1.02	1.18	0.89
53	0.80	20.0	0.50	7.80	7.29	3.44	3.40	1.13	1.30	0.63	1.34	1.05	1.14	1.18	1.12
54	0.80	20.0	1.00	7.59	11.06	4.41	4.22	1.10	1.17	0.48	0.99	0.98	1.00	0.83	0.99
55	0.80	25.0	0.50	9.62	11.78	5.79	4.56	1.13	1.33	0.79	1.25	1.04	1.17	1.09	1.06
56	0.80	25.0	1.00	9.87	17.64	9.26	5.72	1.16	1.18	0.75	0.93	1.03	1.02	0.95	0.94
Max								1.16	1.54	1.04	1.52	1.15	1.18	1.18	1.19
Min								0.72	0.81	0.26	0.87	0.83	0.85	0.83	0.83
Mean								0.91	1.16	0.78	1.16	1.00	1.00	0.99	1.00
COV								0.121	0.145	0.217	0.141	0.074	0.080	0.069	0.095

Table 5

FE results of the SCFs of line D in 56 fabricated box X-joints under chord axial loading.

Joint no.	β	2γ	τ	$SCF_{FE,ch}$	$SCF_{FE,ch}/SCF_{C,ch}$	$SCF_{FE,ch}/SCF_{P,ch}$
1	0.35	12.5	0.25	1.50	1.27	1.09
2	0.35	12.5	0.50	1.60	1.15	1.08
3	0.35	12.5	0.75	1.65	1.07	1.07
4	0.35	12.5	1.00	1.68	1.02	1.06
5	0.35	16.0	0.25	1.41	1.17	1.00
6	0.35	16.0	0.50	1.52	1.07	1.01
7	0.35	16.0	0.75	1.52	0.97	0.97
8	0.35	16.0	1.00	1.53	0.91	0.95
9	0.35	20.0	0.25	1.39	1.14	0.98
10	0.35	20.0	0.50	1.52	1.05	1.00
11	0.35	20.0	0.75	1.52	0.96	0.96
12	0.35	20.0	1.00	1.52	0.89	0.93
13	0.35	25.0	0.25	1.34	1.08	0.93
14	0.35	25.0	0.50	1.46	1.00	0.95
15	0.35	25.0	0.75	1.50	0.93	0.93
16	0.35	25.0	1.00	1.48	0.85	0.89
17	0.50	12.5	0.25	1.58	1.24	1.08
18	0.50	12.5	0.50	1.71	1.14	1.09
19	0.50	12.5	0.75	1.78	1.07	1.09
20	0.50	12.5	1.00	1.74	0.98	1.03
21	0.50	16.0	0.25	1.49	1.14	1.00
22	0.50	16.0	0.50	1.65	1.07	1.03
23	0.50	16.0	0.75	1.67	0.98	1.00
24	0.50	16.0	1.00	1.67	0.91	0.97
25	0.50	20.0	0.25	1.47	1.10	0.97
26	0.50	20.0	0.50	1.61	1.02	0.99
27	0.50	20.0	0.75	1.65	0.95	0.97
28	0.50	20.0	1.00	1.62	0.87	0.93
29	0.50	25.0	0.25	1.42	1.04	0.92
30	0.50	25.0	0.50	1.57	0.97	0.94
31	0.50	25.0	0.75	1.63	0.91	0.94
32	0.50	25.0	1.00	1.63	0.86	0.92
33	0.65	12.5	0.25	1.66	1.21	1.07
34	0.65	12.5	0.50	1.88	1.15	1.13
35	0.65	12.5	0.75	1.93	1.08	1.12
36	0.65	12.5	1.00	1.94	1.01	1.09

37	0.65	16.0	0.25	1.58	1.11	0.99
38	0.65	16.0	0.50	1.76	1.04	1.03
39	0.65	16.0	0.75	1.80	0.97	1.01
40	0.65	16.0	1.00	1.80	0.91	0.99
41	0.65	20.0	0.25	1.57	1.07	0.96
42	0.65	20.0	0.50	1.76	1.02	1.01
43	0.65	20.0	0.75	1.83	0.96	1.01
44	0.65	20.0	1.00	1.83	0.89	0.98
45	0.65	25.0	0.25	1.50	0.99	0.90
46	0.65	25.0	0.50	1.69	0.95	0.95
47	0.65	25.0	0.75	1.75	0.89	0.94
48	0.65	25.0	1.00	1.79	0.85	0.93
49	0.80	12.5	0.25	1.75	1.17	1.06
50	0.80	12.5	0.50	1.93	1.10	1.10
51	0.80	12.5	1.00	2.11	1.02	1.12
52	0.80	20.0	0.25	1.68	1.04	0.96
53	0.80	20.0	0.50	1.94	1.02	1.04
54	0.80	20.0	1.00	2.13	0.95	1.07
55	0.80	25.0	0.50	1.85	0.94	0.96
56	0.80	25.0	1.00	2.06	0.88	1.00
Max					1.27	1.13
Min					0.85	0.89
Mean					1.02	1.00
COV					0.102	0.061

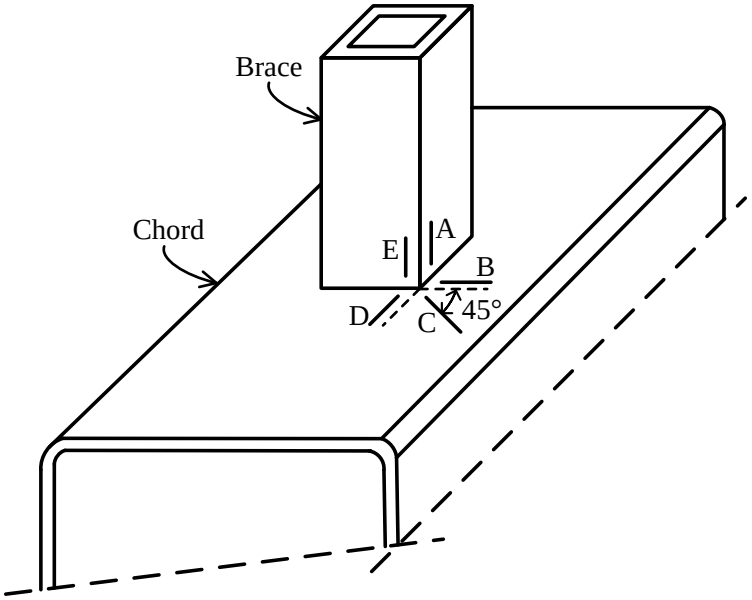

Fig. 1. Hot spot locations for RHS X- and T-joints [4].

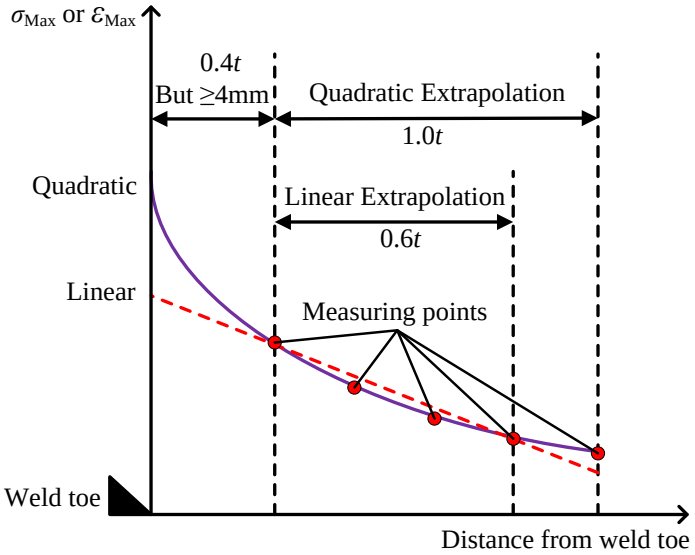

Fig. 2. Extrapolation region and extrapolation methods for hot spot stress method [1].

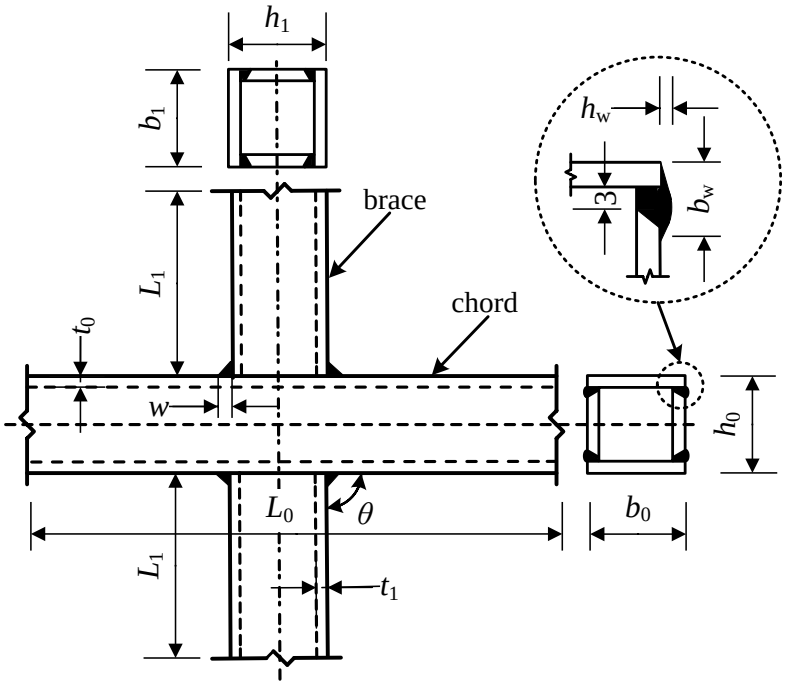

Fig. 3. Configuration and notations of fabricated box X-joints (dimensions in mm).

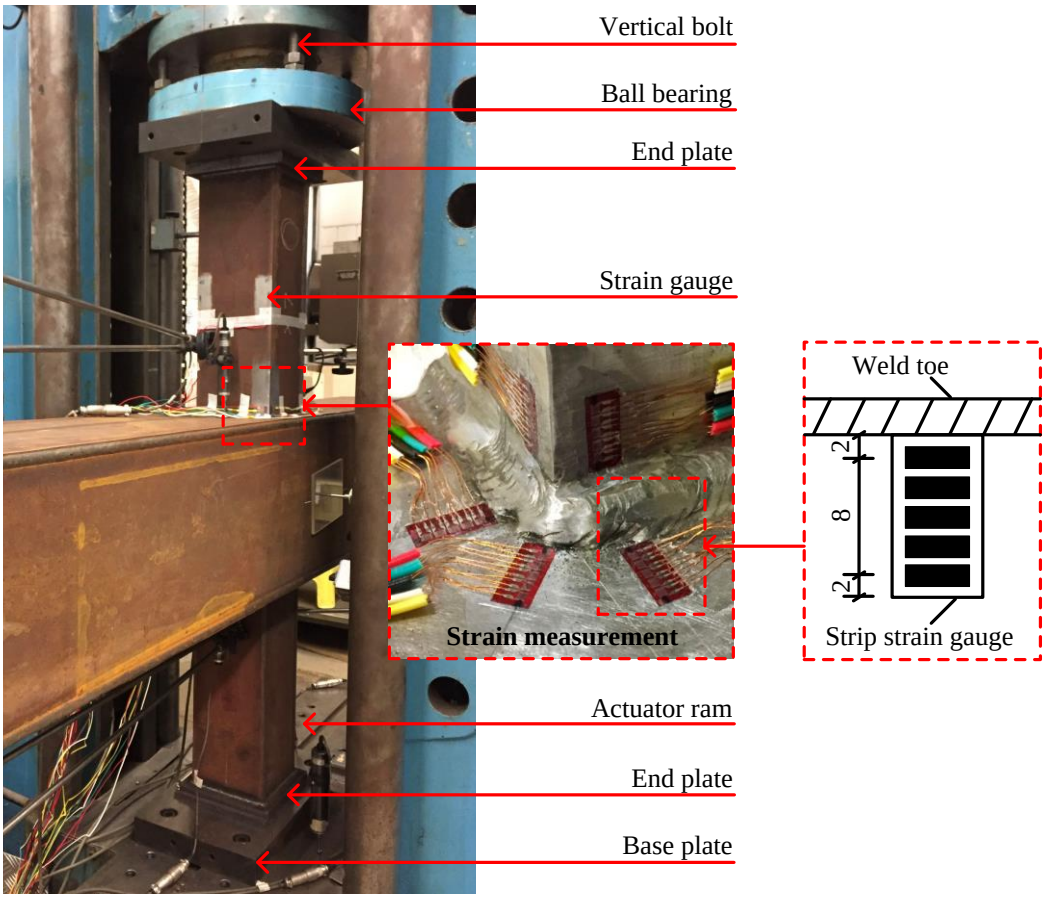

Fig. 4. Test set-up for fabricated box X-joint test specimens.

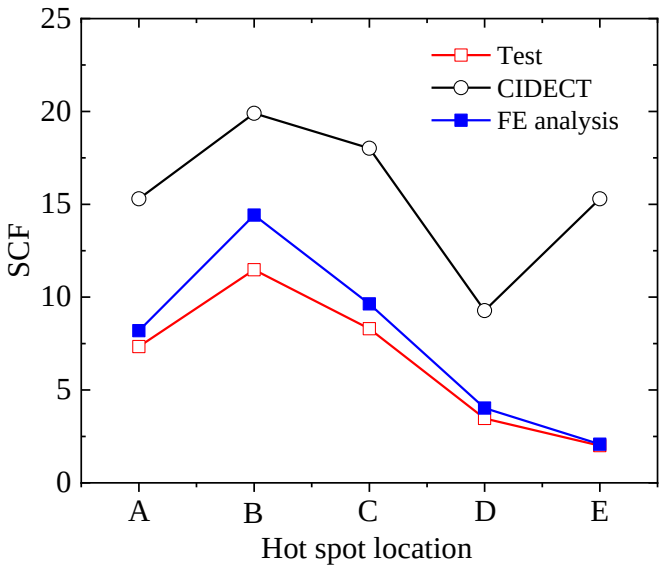

(a) X-C120×6-B60×6

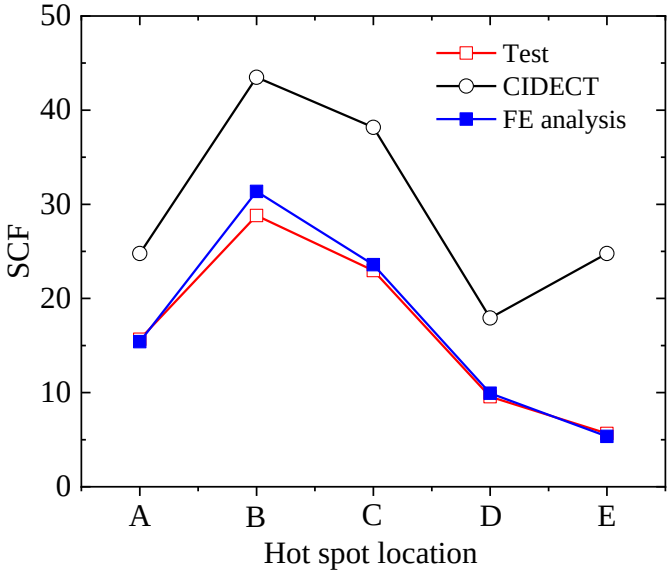

(b) X-C180×6-B90×6

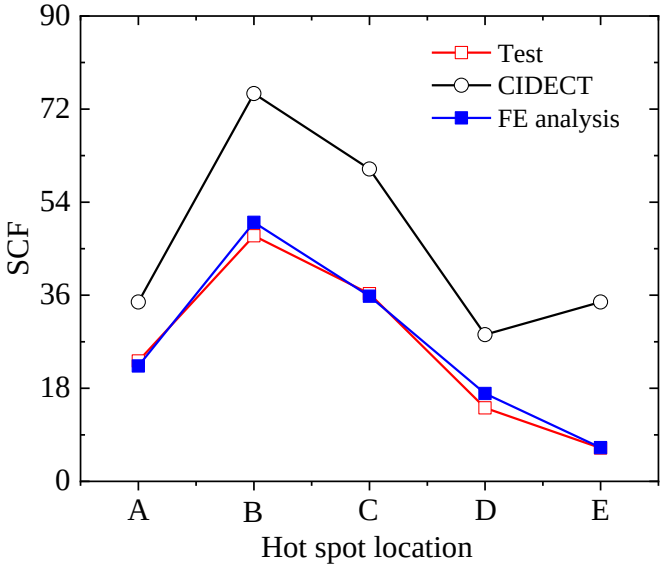

(c) X-C240×6-B120×6

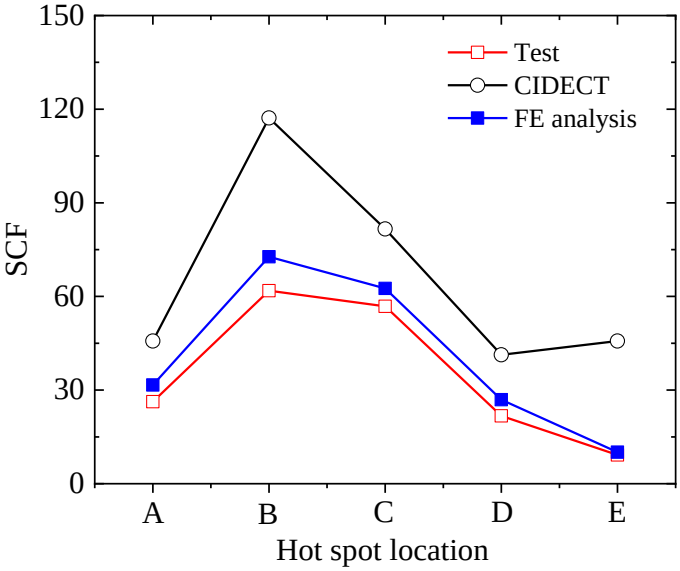

(d) X-C300×6-B150×6

Fig. 5. Comparison of the SCFs obtained from tests, CIDECT SCF formulae and FE analyses.

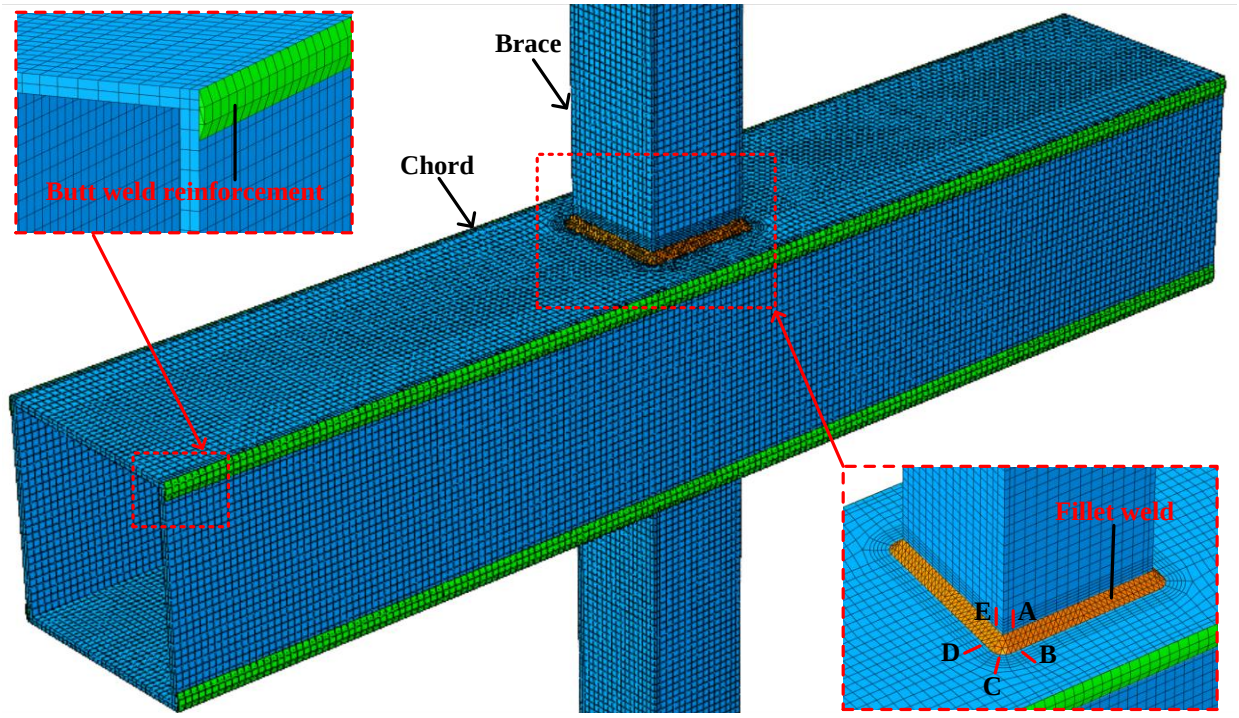

Fig. 6. FE model adopted for validation study.

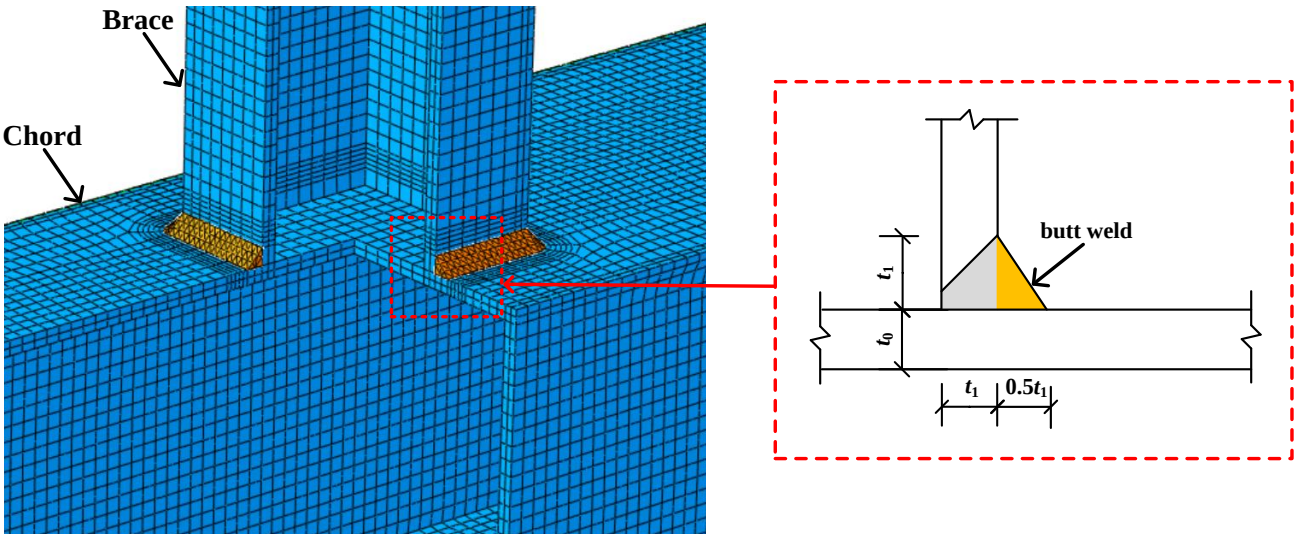

Fig. 7. Profile of the butt weld adopted for parametric study.

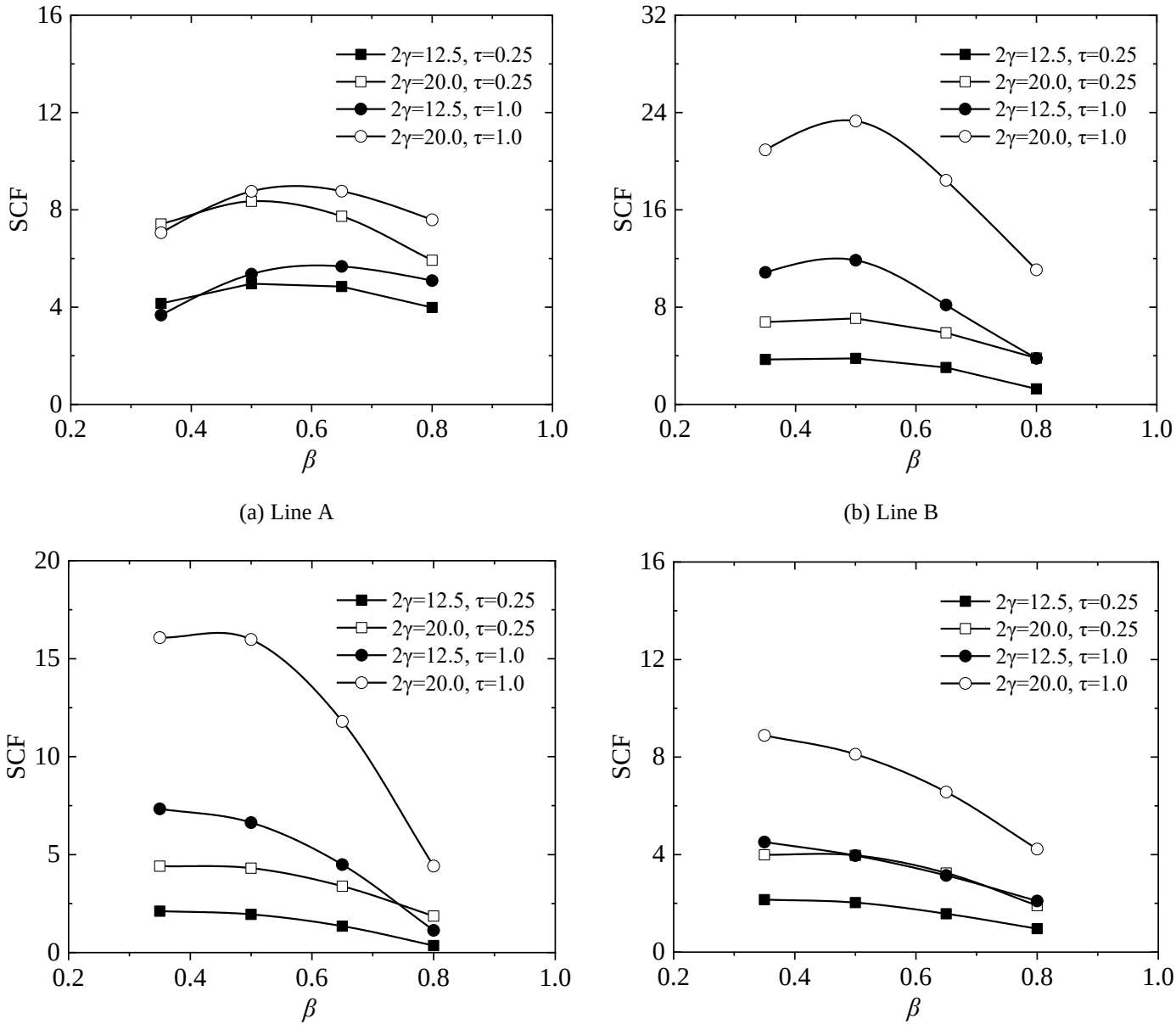

(a) Line A

(b) Line B

(c) Line C

(d) Line D

Fig. 8. Typical SCF distributions of fabricated box X-joints under brace axial loading.

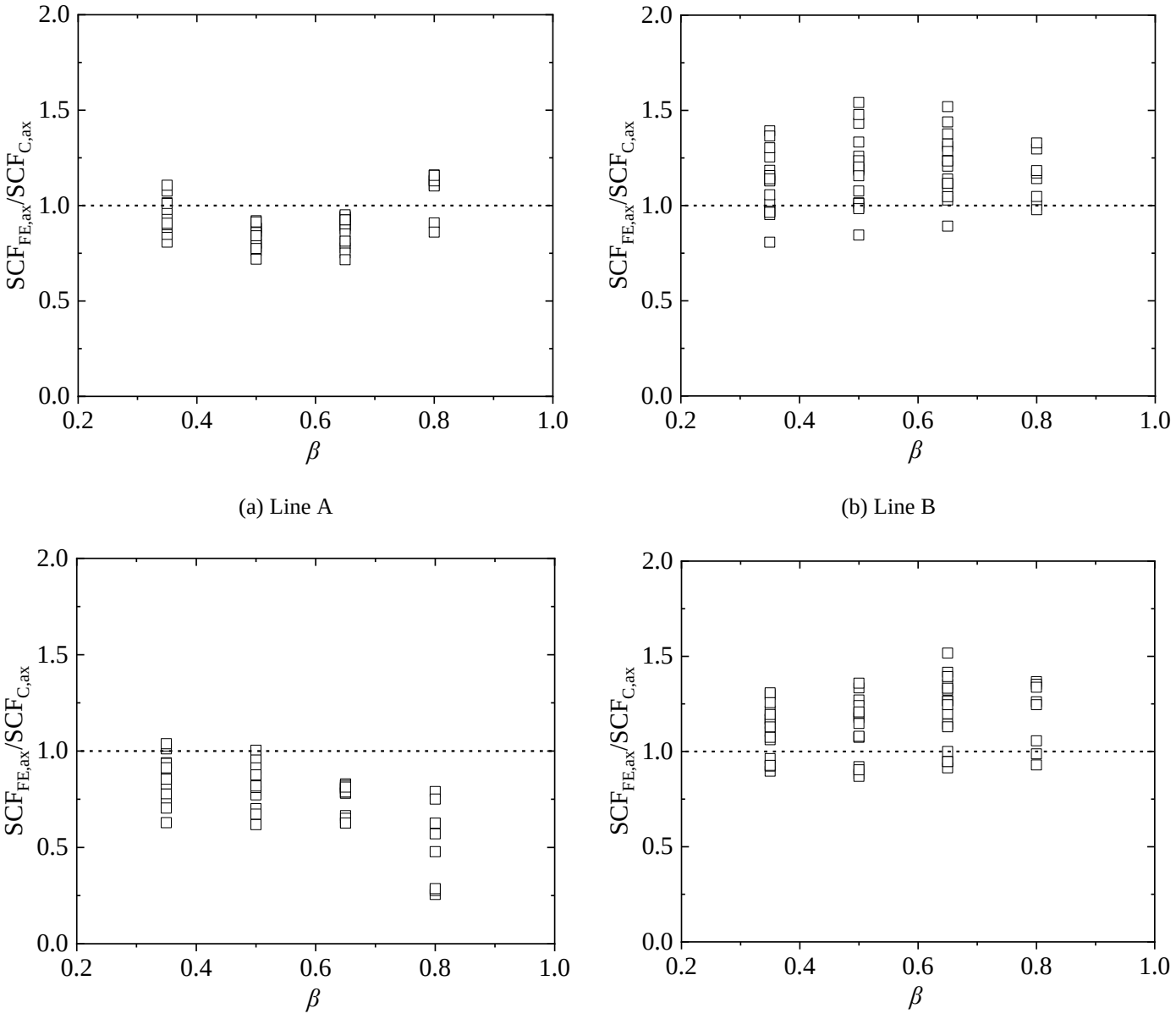

(a) Line A

(b) Line B

(c) Line C

(d) Line D

Fig. 9. Comparison of FE and CIDECT SCFs for brace axial loading.

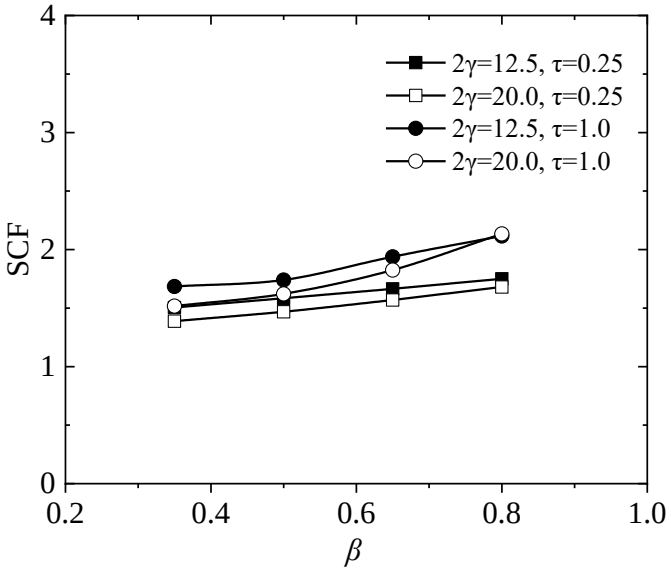

Fig. 10. Representative SCF distributions of Line D in fabricated box X-joints under chord axial loading.

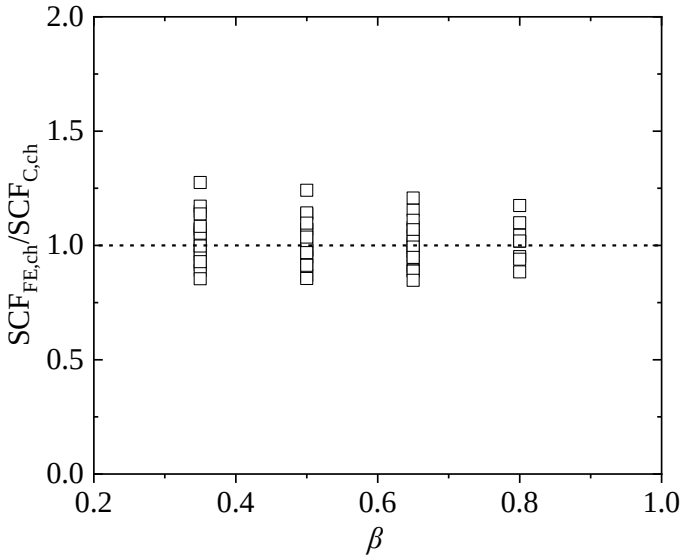

Fig. 11. Comparison of FE and CIDECT SCFs of line D for chord axial loading.

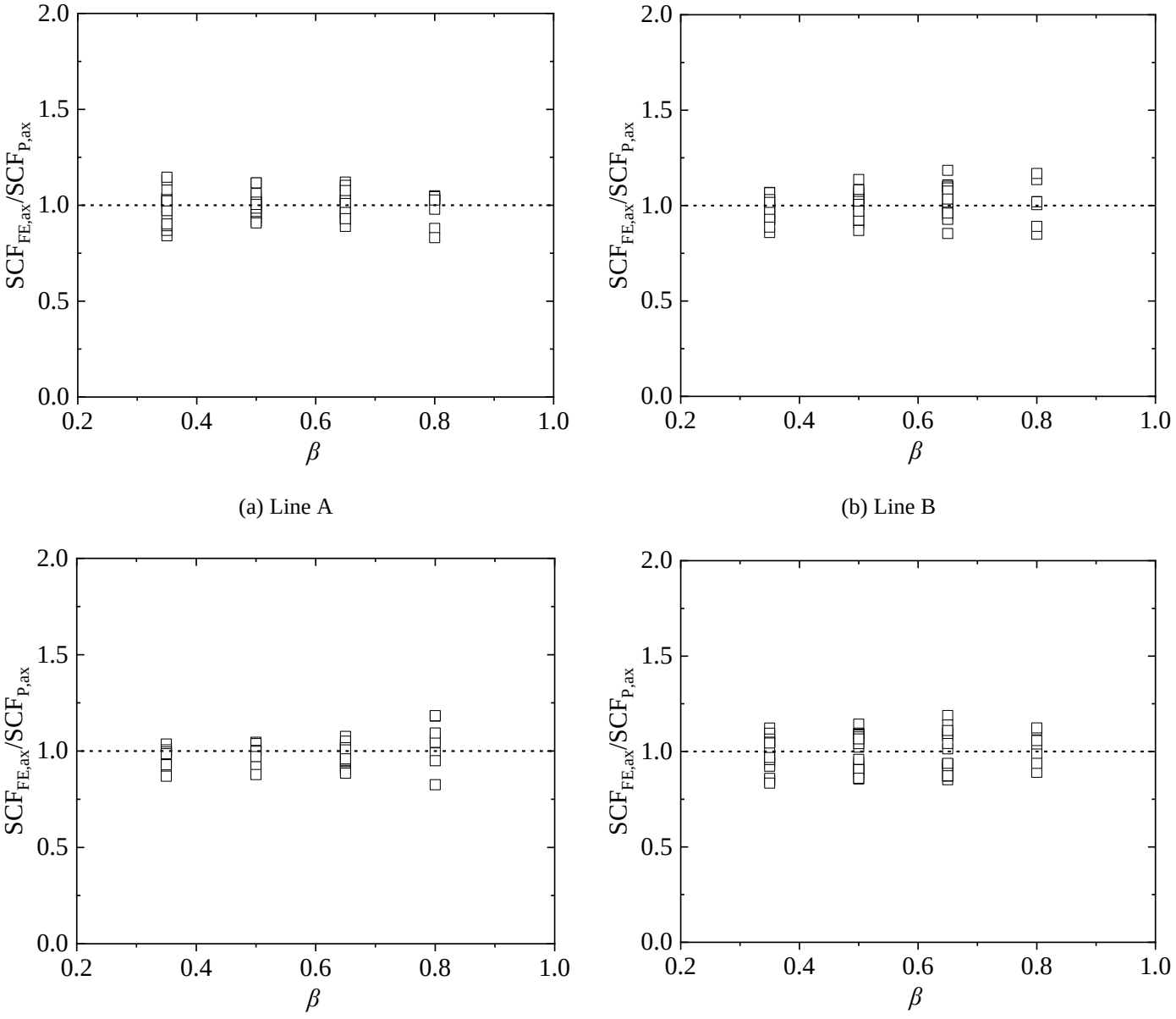

(a) Line A

(b) Line B

(c) Line C

(d) Line D

Fig. 12. Comparison of FE and proposed SCFs for brace axial loading.

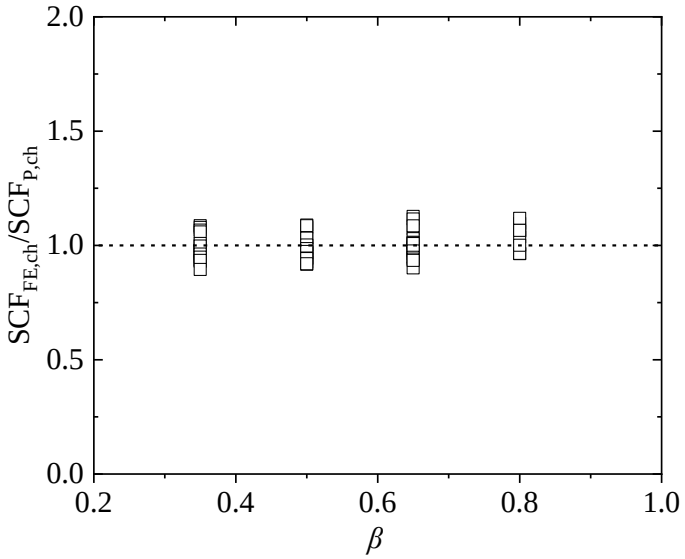

Fig. 13. Comparison of FE and proposed SCFs of line D for chord axial loading.